ACS APPLIED NANO MATERIALS

www.acsanm.org Article

Functionalized Carbon Nanoparticle-Based Sensors for Chemical Warfare Agents

Nunzio Tuccitto,* Lorenzo Riela, Agatino Zammataro, Luca Spitaleri, Giovanni Li-Destri, Gianfranco Sfuncia, Giuseppe Nicotra, Andrea Pappalardo, Giacomo Capizzi, and Giuseppe Trusso Sfrazzetto*

Cite This: *ACS Appl. Nano Mater.* 2020, 3, 8182–8191 Read Online

ACCESS | Metrics & More | Article Recommendations | Supporting Information

ABSTRACT: Real-time sensing of chemical warfare agents (CWAs) is, today, a crucial topic to prevent lethal effects of a chemical terroristic attack. For this reason, the development of efficient, selective, sensitive, and reversible sensoristic devices, which are able to detect by optical response the ppm levels of these compounds, both in water and in air, is strongly required. Here, we report the design and synthesis of a fluorescent nanosensor, based on carbon nanoparticles covalently functionalized with ethanolamine arms, which exploits the multitopic supramolecular interaction with nerve agents, ensuring highly efficient (log K 6.46) and selective molecular recognition. Moreover, given the aqueous dispersibility of carbon nanoparticles, these nanosensors ensure even higher sensitivity, detecting sub-ppt concentration of nerve agents in water, and sub-ppm level in air by using a common digital camera or a smartphone. Our results pave the way to an innovative class of low-cost reusable CWA sensors, prompting, for the first time, the simultaneous detection of nerve agents through gaseous and aqueous media, thus extending the protection range to public water supplies.

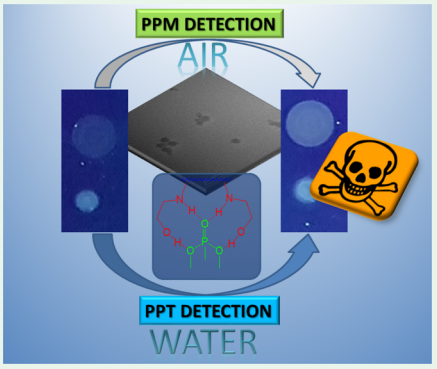

KEYWORDS: *nanosensor, chemical warfare agents, supramolecular sensor, carbon nanoparticles, multi-topic approach*

1. INTRODUCTION

Nerve agents are a group of highly toxic organophosphorus compounds developed during World War II. They are related to organophosphorus pesticides though they have a much higher human acute toxicity than commonly used pesticides. Because of their high toxicity, these nerve agents have been used as chemical weapons and for these reasons are today called chemical warfare agents (CWAs). CWAs are classified into three main classes: G-type, V-type, and the most recently A-type (also called Novichok) (Chart 1).

Although CWAs are outlawed and prohibited in many countries, the recent terrorist attacks in the Middle East and also in Europe highlight the importance to quickly detect, in real time, the presence of these agents.[1,2]

Toxicity levels of most used CWAs are in the ppm-sub ppm range.[3] In particular, the LC50 (air concentration level of the chemical that kills 50% of the test animals) of Tabun and Sarin is 2 and 1.2 ppm, respectively, while Soman and VX have LC50 of 0.9 and 0.3 ppm, respectively.[3] Thus, the necessity to obtain a real practical sensor for the detection of these low concentration values of CWAs is huge.

For security reasons, the use of CWAs is not permitted for research activity; thus, the development of new and more efficient sensors and relative recognition studies can only be performed by using simulants, less toxic compounds having similar geometric structures but different reactivities.[4] In particular, dimethyl methylphosphonate (DMMP) is widely recognized as one of the best simulant for G-type CWAs. In particular, G and V-Type CWAs have two common features: (i) the presence of a Lewis Base site (P═O) and (ii) the presence of two hydrogen bond acceptor groups covalently linked to the phosphorous atom. These characteristics can be found also in DMMP.

Traditionally, the detection of G- and V-type CWAs is based on a "covalent approach", in which a covalent reaction occurs between the sensor and the analyte, leading to the formation of a new compound having different properties with respect to the starting sensor.[5] In particular, detection methods based on spectroscopic measurements (e.g., optical measurements, such as absorbance or fluorescence) are cheap and convenient, due to the fast and clear visible response to the presence of the given analyte.[6]

However, the covalent approach suffers from many limits: (i) it is not specific for the analyte, due to the possibility to

Received: June 10, 2020
Accepted: July 16, 2020
Published: July 16, 2020

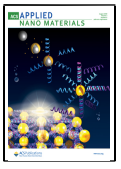

https://dx.doi.org/10.1021/acsanm.0c01593
ACS Appl. Nano Mater. 2020, 3, 8182–8191

Chart 1. Structures and Names of G-Type, V-Type, and General Formula of A-Type CWAs

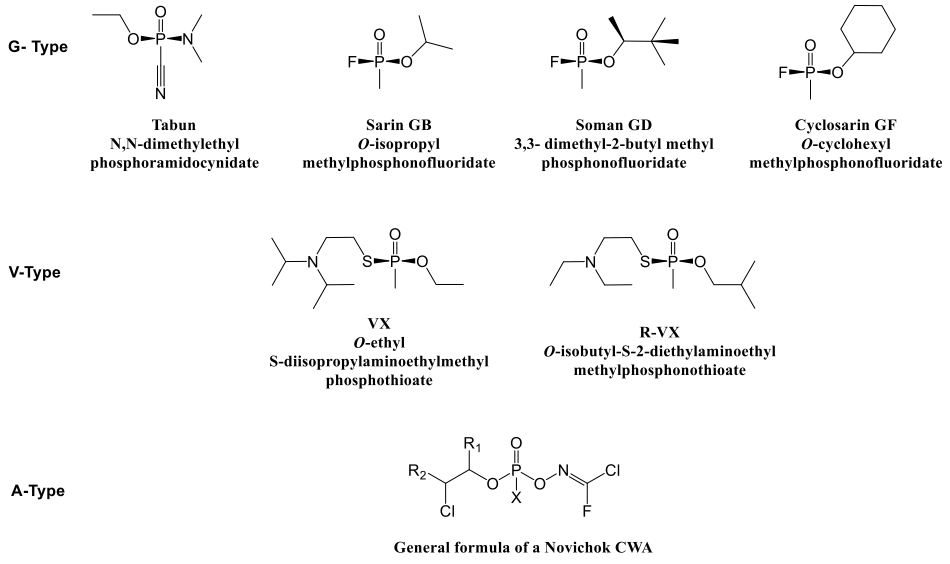

Scheme 1. Top: Representation of Naphthyl-di-AE, CNPs-C_2-OH, and DMMP Chelation Mechanism; down: Synthesis of CNPs-C_2-OH

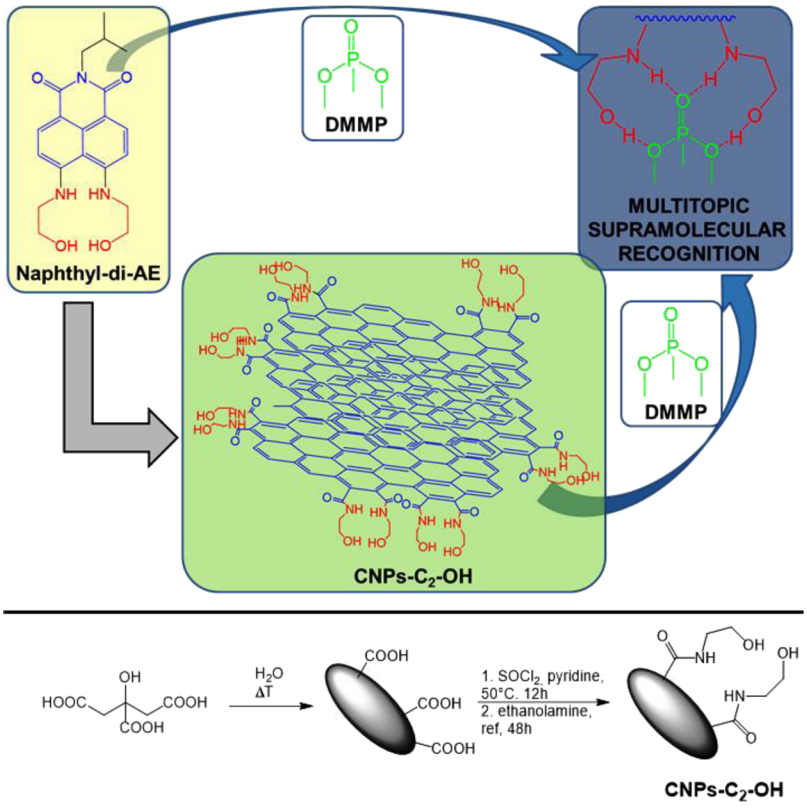

react with other substances; (ii) the low selectivity can lead to false-positive responses; and (iii) these sensors cannot be reused after the exposure to the analyte.

Recently, the alternative supramolecular approach has been proposed.[7] This strategy is based on the formation of noncovalent interactions between the receptor and analyte, leading to a reversible but stable interaction. The goal of the supramolecular approach is to give alternative pathways with respect to the traditional chemical reactivity, minimizing or eliminating the effects of the presence of competitive analytes and realizing a reusable sensor.[8−17]

In this context, by taking advantage of the most recent findings in the field of supramolecular chemistry,[18−21] our research group proposed to build, with a 'bottom-up' approach, sensing devices for the noncovalent detection of CWA molecules via a "multitopic approach".[22−24] In particular, our target is to recognize CWAs *via* noncovalent reversible interactions, involving different recognition sites (multitopic) of the analyte. The possibility to simultaneously recognize two

https://dx.doi.org/10.1021/acsanm.0c01593
ACS Appl. Nano Mater. 2020, 3, 8182−8191

or more sites of the analyte leads to highly efficient and selective sensors, thus avoiding false-positive responses.

The main limitation of the above described systems was the poor solubility in water, thus precluding the possibility to detect traces of CWAs in water. Unfortunately, the risk of water contamination in a terrorist attack is high, and the potential lethal effects on the human population are huge. In fact, most of the Nerve Agents are water soluble and can be rapidly dissolved. Thus, they could be used to poison water or food, or can be easily nebulized in air. In this context, while the detection of Nerve Agents in the gas phase can be performed by a solid device, their detection in aqueous environments is still unattained, thus leaving a substantial safety issue related mainly to the contamination of public water supplies.

For all these reasons, the development of efficient selective sensors that are able to detect traces (ppm or sub-ppm) of Nerve Agents in water (monitoring hydraulic systems or food/drink) and in the gas phase (environmental monitoring of the atmosphere) is, today, a primary target for the human security, precluding the lethal effect of a terrorist attack using CWAs.

For these reasons, our attention has been focused on carbon nanoparticles. These nanostructures show interesting properties, such as high water solubility, high fluorescence emission, the possibility to tune the emission by depending on the chemical composition of the external shell. In addition, the possibility to covalently functionalize the external shell leads to a wide range of application.

Here, we describe a new water-soluble CWA sensor, **CNPs-C_2-OH** (Scheme 1), based on functionalized carbon nanoparticles, is able to detect traces of DMMP in water (ppt levels) and sub-ppm concentrations in the gas phase. To the best of our knowledge, it is the first example of a water-soluble CWA sensor simultaneously working in aqueous and gas media. Moreover, thanks to the high fluorescent quantum yield of carbon nanoparticles and the supramolecular interaction between the nanosensor and nerve agents, the sensor described here requires a very low amount of active materials and is reusable. Therefore, its implementation in security systems is affordable and long lasting.

2. EXPERIMENTAL SECTION

2.1. General Experimental Methods. The NMR experiments were carried out at 27 °C on a Varian UNITY Inova 500 MHz spectrometer (^{1}H at 499.88 MHz, ^{13}C NMR at 125.7 MHz) equipped with a pulse-field gradient module (*Z* axis) and a tunable 5 mm Varian inverse detection probe (ID-PFG). Luminescence measurements were carried out using a Cary Eclipse Fluorescence spectrophotometer at room temperature. The emission was recorded at 90° with respect to the exciting line beam, using 5:5 slit widths for all measurements. All chemicals were reagent grade and used without further purification. Atomic force microscopy (AFM) images were obtained with a Nanoscope IIIa apparatus from Digital Instruments (Santa Barbara, CA) operated in tapping mode in air. Tap 300G silicon probes from Budget Sensors with a nominal resonance frequency of 300 kHz were used. The transmission electron microscopy (TEM) investigation was performed with a JEOL ARM200F Cs-corrected microscope, equipped with a cold-field-emission gun with an energy spread of 0.3 eV and operating at 200 keV. Micrographs were acquired in Conventional TEM (CTEM) mode using a Gatan UltraScan 1000XP (2k × 2k) charge coupled device camera, with low electron fluence in order to reduce the beam damage. The TEM sample was prepared by depositing a drop of the nanoparticle's dispersion on a TEM grid having an ultrathin carbon film (<3 nm), ideal for TEM imaging of low contrast particles. X-ray photoelectron spectra (XPS) were measured at a 45° take-off angle relative to the surface normal with a PHI 5600 Multi Technique System (base pressure of the main chamber 3 × 10^{-8} Pa).[25,26] Samples were excited with the Al Kα X-ray radiation using a pass energy of 5.85 eV. Structures due to the Kα satellite radiations were subtracted from the spectra prior to data processing. Spectra calibration was achieved by fixing the C 1s signal at 285.0 eV.[25,26] The instrumental energy resolution was ≤0.5 eV. The XPS peak intensities were obtained after Shirley background removal.[25,26] The atomic concentration analysis was performed by taking into account the relevant atomic sensitivity factors. The fittings of the C 1s, N 1s, and O 1s XP spectra were carried out using Gaussian envelopes after the subtraction of the background until there was the highest possible correlation between the experimental spectrum and the theoretical profile. The residual or agreement factor *R*, defined by $R = [\sum(F_{obs} - F_{calc})^2/\sum(F_{obs})^2]^{1/2}$, after minimization of the function $\sum(F_{obs} - F_{calc})^2$, converged to the value of 0.03. Samples for XPS measurement were deposited on silicon substrates. Fourier-transform infrared (FTIR) spectra were recorded from 1000 to 4000 cm^{-1} with a PerkinElmer spectrometer; pure and functionalized CNPs were mixed with potassium bromide (KBr) and then pressed into pills.

2.2. Synthesis of CNPs-C_2-OH. Native CDs (100 mg)[27] were mixed with 20 mL of thionyl chloride (274 mmol) and 500 μL of pyridine under N_2. The reaction was heated at 50 °C overnight. Then, 500 mg (8.20 mmol) of ethanolamine were added and the reaction mixture was refluxed for 48 h under a nitrogen atmosphere. The reaction was cooled to room temperature and rotovaporated under vacuum to remove volatile compounds. Excess of ethanolamine, and other undesired products, was removed by dialysis (11,000 Da cut-off). ^{1}H NMR (500 MHz, D_2O) δ 3.25 (t, J = 5.5 Hz, 2H), 2.99 (t, J = 5.5 Hz, 2H).

2.3. Procedure for Fluorescence Titrations. Two mother solutions of the host (0.05 mg/mL) and guest (1.0 × 10^{-5} M) in water were prepared. From these, different solutions with different DMMP volume (0, 0.2, 0.5, 1.0, 1.5, 2.0, 2.5, 5.0, 7.0, 10.0, 15.0, 20.0, 50.0, 70.0, 100.0, and 150.0 μL) were prepared, and the emission spectra were recorded at 25 °C. Fluorescence titration was performed by using λ_{ex} 300 nm, recording the emission values at 406 nm. The apparent binding affinities of **CNPs-C_2-OH** with DMMP were estimated using HypSpec (version 1.1.33),[28−31] a software designed to extract equilibrium constants from potentiometric and/or spectrophotometric titration data. HypSpec starts with an assumed complex formation scheme and uses a least-squares approach to derive the spectra of the complexes and the stability constants. χ^2 test (chi-square) was applied, where the residuals follow a normal distribution (for a distribution approximately normal, the χ^2 test value is around 12 or less). In all of the cases, $\chi^2 \leq 10$ were found, as obtained by 3 independent measurements sets. The limit of detection was calculated by the method of the calibration curve using the formula DL = 3 s/K, where s is the standard deviation of the blank and K is the slope of the calibration curve. The estimated Φ_F value of **CNPs-C_2-OH** is 0.32, calculated by using *N*-butyl-4-butylamino-1,8-naphthalimide as a standard (Φ_F = 0.81).[32]

2.4. Procedure for Test Strip. Two microliters of a solution of **CNPs-C_2-OH** (0.05 mg/mL in water) and unfunctionalized carbon nanoparticles (0.05 mg/mL in water) were adsorbed onto several neutral alumina foils (1.5 × 3.5 cm) and the solvent was removed under nitrogen flow. Each of these solid samples were inserted into a vial (23 mL) containing different amounts (0, 0.2, 0.5, 0.7, 1.0, 2.0, 5.0, 10.0, 20.0, 30.0, 50.0, 60.0, 70.0, 80.0, 90.0, and 100.0 μL) of DMMP. All vials were maintained at 50 °C for 1 h in an oven. This temperature and time were selected in order to guarantee the presence of DMMP in the gas phase (at 25 °C, volatility of DMMP is 3 times lower). After this time, the foil was observed under a UV−vis lamp at 365 nm. The vapor concentration of DMMP was calculated by considering the volatility of DMMP (60,570 mg/m^3 at 50 °C),[33] and the total volume of the vial used for the Test Strip (23 mL).

2.5. Automatic Image Processing Methods. We selected the region of interest related to the spot from the pictures and we normalized the gray level images intensity I (vide infra, see Figure 6c) according to the following equation

https://dx.doi.org/10.1021/acsanm.0c01593
ACS Appl. Nano Mater. 2020, 3, 8182−8191

$$I_N = \frac{(I - \min(I)) \times 255}{(\max(I) - \min(I))} \quad (1)$$

Normalizing with respect to the maximum value of the average luminance I_{Ni}, we obtain the set of experimental data points $(An_i, \overline{\mu l}_i)$ where $0 \le \overline{\mu l} \le 1$. Starting from such a set of experimental data points $(An_1, \overline{\mu l}_1)$, $(An_2, \overline{\mu l}_2)$, ..., $(An_m, \overline{\mu l}_m)$, we obtained a curve that is the "best fit" for the data in the least-squares sense as the normal and useful practice used in many applications in statistics, engineering, and other applied sciences. More precisely given the set of discrete data points $(An_i, \overline{\mu l}_i)$, $i = 1, 2, ..., m$. Find the algebraic polynomial

$$P_N(\overline{\mu l}) = a_0 + a_1\overline{\mu l} + a_2\overline{\mu l}^2 + \cdots + a_N\overline{\mu l}^N \qquad (N < m) \quad (2)$$

such that the error $E(a_0, a_1, ..., a_N)$ in the least-squares sense in minimized, that is

$$E(a_0, a_1, ..., a_N) = \sum_{i=1}^{m} (An_i - a_0 - a_1\overline{\mu l}_i - a_2\overline{\mu l}_i^2 - \cdots - a_N\overline{\mu l}_i^N)^2 \quad (3)$$

is minimum. Here, $E(a_0, a_1, ..., a_N)$ is a function of $(N + 1)$ variables: $a_0, a_1, ..., a_N$. After the minimization of this function, we obtain a system of $(N + 1)$ equations in $(N + 1)$ unknowns $a_0, a_1, ..., a_N$. These equations are called normal equations.

The above system has the form

$$V^T V\overline{a} = b \quad (4)$$

where

$$\overline{a} = \begin{bmatrix} a_1 \\ \vdots \\ a_N \end{bmatrix} \quad (5)$$

The matrix V is the Vandermonde matrix. Because in our case values $\overline{\mu l}_i$ are distinct, the system has a unique solution (Theorem of Existence and uniqueness of Discrete Least-Squares Solutions). In order to find the "best fit" for the data, we have used 16 normalized experimental data points ($m = 16$) and a polynomial of order 10 ($N = 10$). By analyzing the coefficients of the polynomial obtained with the solution of eq 3, we noticed that these coefficients coincide (unless approximation errors) with the coefficients of the series expansion of the function

$$A_N(\overline{\mu l}) = 1 - e^{-\alpha \cdot \overline{\mu l}} \quad (6)$$

3. RESULTS AND DISCUSSION

3.1. Design, Synthesis, and Characterization. This new nanosensor was designed starting from our recent fluorescent probe Naphthyl-di-AE (Scheme 1).[23] In particular, we demonstrated how the presence of ethanolamine arms leads to an efficient supramolecular binding of DMMP, by the formation of multiple hydrogen bonds (Scheme 1). Naphthyl-di-AE was constituted by a chelating group (ethanolamine arms, in red in Scheme 1-top) and an aromatic fluorescent scaffold (Naphthyl-diimide scaffold, in blue in Scheme 1-top). Therefore, in the present work we extended the fluorescent moiety, exploiting the emission properties of carbon nanoparticles, associated with the proximity effect of the nanostructure, which should lead to an amplification effect. In addition, the presence of multiple alcoholic groups on the nanoparticle surface leads to a water-soluble organic nanostructure.

In details, **CNPs-C_2-OH** has been designed to exploit the recognition properties of ethanolamine arms,[23] also improving the solubility in water.

Carbon nanoparticles (CNPs) are a new class of carbon nanomaterials, having characteristic photochemical and redox properties.[34] These nanomaterials are about 10 nm in diameter, with a quasi-spherical shape. They are characterized by high optical and chemical stability, good water solubility, photobleaching resistance biocompatibility, and low-cost preparation. For these reasons, nowadays CNPs found application in a wide range of fields, such as analytical chemistry,[35] biosensing,[36] bioimaging,[37] theranostics,[38] molecular communication,[39] and photocatalytic energy conversion.[40]

Our strategy is to combine the recognition properties offered by the "multitopic approach" with the water solubility and the excellent optical properties of CNPs, in order to obtain a new generation of nanostructured water-soluble sensors for the efficient and selective detection of CWAs in water and gas phases. In the proposed nanosensor, in fact, the multitopic recognition site is due to the presence of ethanolamine arms, which is able to interact with the CWA simulant by exploiting multiple hydrogen bonds (see Scheme 1-top). This H-bond configuration guarantees high selectivity, reducing the possibility to false-positive responses. The synthesis of **CNPs-C_2-OH** is reported in Scheme 1-down.

One of the main advantages of the carbon nanoparticles is the easy preparation. In particular, the starting material is citric acid. To covalently functionalize the nanoparticle surface, we considered the nanoparticle surface as a simple carboxylic acid. In fact, after thermal treatment in water, citric acid leads to carboxy-terminal CNPs,[27] which have been activated by using thionyl chloride into the relative acylic chlorides. In the presence of an excess of ethanolamine, the **CNPs-C_2-OH** can be easily obtained (see the Experimental section). Functionalized nanoparticles have been purified by dialysis, and they have been chemically characterized by ^{1}H NMR and XPS, confirming the covalent functionalization of the surface (see Supporting Information).

In particular, the ^{1}H NMR spectrum in D_2O of **CNPs-C_2-OH** shows two triplet signals having different chemical shifts with respect to the ethanolamine protons (see Supporting Information, Figure S2), supporting the covalent reaction between nanoparticles and the ethanolamine.

CTEM investigation was performed to obtain a statistical distribution of nanoparticle diameters. More than 650 nanoparticles were analyzed, and an average diameter of 16.4 ± 7.6 nm was obtained. Figure 1 reports a TEM image of nanoparticles. Diameter distribution was fitted with a Gaussian distribution peaked at 14.1 nm (inset of Figure 1).

Accurate AFM analysis shows isolated carbon dots without any tendency to aggregate (see Supporting Information, Figure S3). The section analysis characterization reveals polydispersity on both dot diameter and height (see Supporting Information, Figure S3). In particular, the height distribution, ranging from sub-nanometer to few nanometers, indicates a disk-like shape of such organic nanostructures lying on the substrate. As the typical thickness of a graphene layer is 0.4 nm, the measured heights reveal that carbon dots are formed by few or by few tens of graphene-lake flakes.

In order to verify the chemical composition of these functionalized nanoparticles, thus confirming the presence of ethanolamine arms onto the surface, extended X-ray photoelectron spectroscopy (XPS) characterization was performed. In particular, the electronic structure of the functionalized nanoparticles provides important information on the chemical environment.[41−43]

https://dx.doi.org/10.1021/acsanm.0c01593
ACS Appl. Nano Mater. 2020, 3, 8182−8191

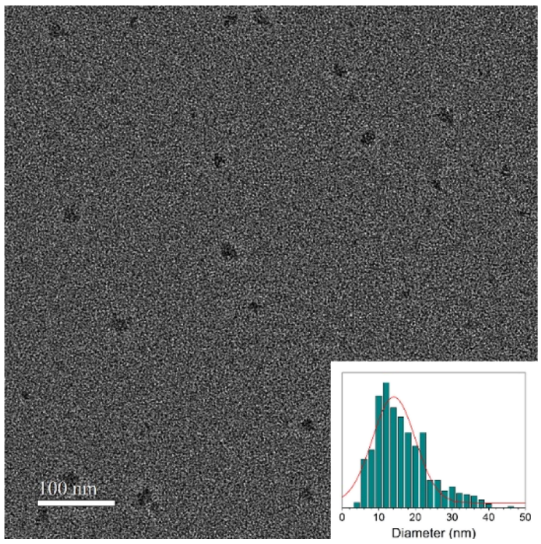

Figure 1. TEM image of nanoparticles. Inset shows the Gaussian fitted diameter distribution.

Figure 2a shows the high-resolution XP spectrum of the **CNPs-C_2-OH** sample in the C 1s binding energy region. An accurate fitting of this spectrum revealed the presence of four components at 285.0, 285.8, 286.8, and 288.3 eV, respectively. The first component (285.0 eV) is due to both aliphatic and aromatic backbones.[25] The peaks at 285.8 and 287.8 eV are assigned to the C−N and C−OH groups, respectively.[44−46] The peak at 288.3 eV is assigned to the carbon of the amide group (−OC−NH−).[46,47] The presence of this signal confirms the covalent functionalization of the nanoparticles with ethanolamine.

Figure 2b shows the O 1s peaks of the **CNPs-C_2-OH**. The O 1s spectral profile was fitted using two Gaussian components at 531.3 and 532.6 eV. The lower energy peak, located at 531.3 eV corresponds to the oxygen of the O═C−N amide group, and further confirms the covalent functionalization of the nanoparticles with the ethanolamine molecule.[48] The higher energy peak, located at 532.6 eV, is assigned to the −OH groups of both CNPs and ethanolamine molecule.[49,50]

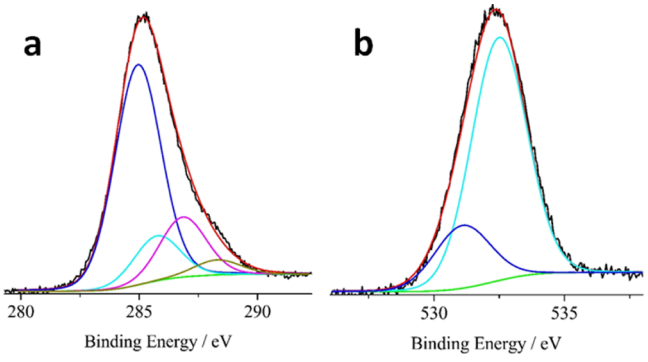

Figure 2. Al Kα excited XPS of **CNPs-C_2-OH** in the (a) C 1s binding energy region: the blue, cyan, magenta, and dark yellow lines refer to the 285.0, 285.8, 286.8, and 288.3 components; the green line refers to the background and the red line superimposed to the experimental black profile refers to the sum of all Gaussian components; (b) O 1s energy region: the black line refers to the experimental profile; the green line refers to the background; the Gaussian at 531.3 (blue line) and that at 532.6 eV (cyan line) represent the two O 1s components; the red line, superimposed to the experimental profile, refers to the sum of the Gaussian components.

Covalent functionalization of nanoparticles was further demonstrated monitoring the XP spectrum of **CNPs-C_2-OH** in the N 1s binding energy region (see Supporting Information, Figure S4). In particular, a band at 400.5 eV in the N 1s region, relative to the amide group (−OC−NH−),[26,46] clearly indicates the covalent link between ethanolamine and carboxylic groups of carbon nanoparticles.

Finally, the XPS probed depth in a carbonaceous material, measured at a 45° take-off angle relative to the surface normal, is about 45 Å. The XPS atomic concentration analysis performed on the carbon nanoparticles functionalized with ethanolamine suggests a high surface coverage, with the nitrogen relative intensity 13.3%, confirming the actual reaction of ethanolamine with the functional groups of the nanoparticle surface.[51]

Also the FTIR analysis of **CNPs-C_2-OH** confirmed the covalent functionalization with ethanolamine arms as revealed by the bands in the region 1000−1250 cm-1 assigned to the C−N stretching (see Supporting Information, Figure S5) with respect to the unfunctionalized carbon nanoparticles.

3.2. Sensing Studies. Sensing studies were performed in water by fluorescence titrations. In particular, we explored the possibility to recognize DMMP in a concentration range of 10^{-9} M to 10^{-6} M in pure water, by using **CNPs-C_2-OH** (0.05 mg/mL). By excitation at 300 nm, nanoparticles show an emission band centered at 406 nm, which undergoes an intensity decrease upon the addition of progressive amounts of DMMP, probably due to a photoinduced electron transfer (PET) mechanism (Figure 3).[52] A nonlinear curve fit of these data indicates a binding constant affinity of log 6.46 ± 0.09, thus suggesting that the presence of multiple chelating arms on the nanoparticle surface leads to an increase of the affinity toward DMMP (if compared to the relative sensor having only two arms).[23,53]

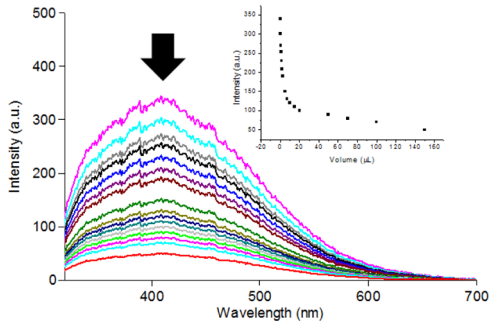

Figure 3. Fluorescence intensity titration of **CNPs-C_2-OH** (0.05 mg/mL in water, λ_{ex} 300 nm) upon the DMMP additions (0.01 mM stock solution); the inset shows the intensity decreases at 406 nm upon the progressive addition of DMMP).

We have designed an organic nanostructure that is able to selectively recognize warfare agents in the aqueous environment by exploiting a fluorescence detection mechanism based on the emission quenching. The motivation for this strategic choice lies in the awareness that the law of exponential decay with the analyte concentration allows for a greater variation at lower concentrations. Indeed, notably, the detection limit calculated for this sensor in the water solution is 0.39 ppt, which is so far the lowest reported value. Considering that, the

https://dx.doi.org/10.1021/acsanm.0c01593
ACS Appl. Nano Mater. 2020, 3, 8182−8191

LC50 levels of G-Type CWAs is in the range 0.3−2 ppm,[3] our sensor is able to detect, in the water solution, a lower order of magnitude of CWAs with respect to the lethal dose.

Selectivity is one of the crucial parameters for *in operando* conditions of a sensor. In this context, the classical CWA probes are based on covalent reactions between a nucleophilic substituent on the sensor scaffold and a given nerve agent simulant. These reactions can lead to false-positive responses because of the low specificity of the reactions itself. By contrast, the success of the multitopic supramolecular approach is based on the formation of reversible noncovalent interactions with two or more sites of the guest, thus leading to higher selectivity and reducing the possibility of a false-positive response. Thus, the air mixture (containing 24,000 ppm of water, 400 ppm CO_2, 5 ppm NO, and 10 ppm CO) was bubbled for 30 min into a 0.05 mg/mL in the water solution of **CNPs-C_2-OH**. The fluorescence spectra of the sensor were acquired before and after air bubbling. Both spectra are superimposable (see the Supporting Information, Figure S6), thus demonstrating that the emission profile of **CNPs-C_2-OH** does not change in the presence of standard analytes/contaminants contained in air (Figure 4). Furthermore,

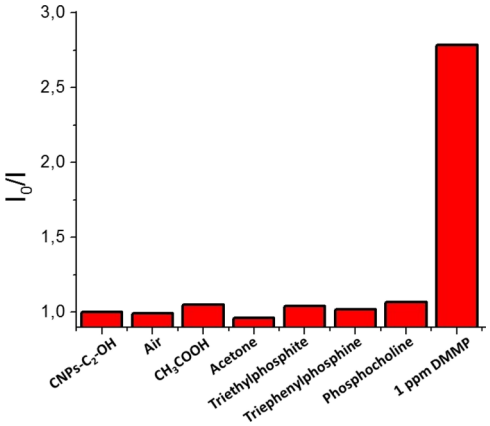

Figure 4. Normalized fluorescence responses of **CNPs-C_2-OH** (0.05 mg/mL in water, λ_{ex} 300 nm) to air (bubbled for 30 min), various competitive guests (50 ppm of acetic acid, acetone, triethylphosphite, triphenylphosphine, and phosphocholine) and DMMP (1 ppm). Bars represent the initial over the final emission intensity at 406 nm.

selectivity of **CNPs-C_2-OH** was tested also by using acetic acid, acetone, and other organophosphorus compounds, such as triethylphosphite, triphenylphosphine, and phosphocholine, as competitors. The addition of 50 ppm of these analytes does not change the emission profile of the nanosensor (Figure 4). Then, 1 ppm of DMMP was added to this air-saturated sensor solution, also containing acetic acid and acetone, observing a clear decrease of the emission intensity, according to the titration described before. These data confirm that the presence in the same arms of NH and OH groups, separated by 2 methylene carbon atoms, allows a perfect distance to bind DMMP both to the P═O and to the O−CH_3. These results confirm the high selectivity of **CNPs-C_2-OH** toward DMMP, in real atmospheric conditions and also in the presence of other competitive analytes. Furthermore, the presence in the air of acid or basic conditions (due to traces of H_2S or NH_3 in the gas phase) should not interfere with the response of the nanosensor. In fact, we demonstrated that acetic acid does not change the emission of **CNPs-C_2-OH**. While alcoholic groups need a strong base, which is difficult to obtain in the gas phase, to be deprotonated; thus, modifying the recognition process.

We note that the nanosensor can differ from the ideal geometry reported in the case of Naphtyl-di-AE. In fact, we do not exclude the interaction of only one ethanolamine arm with DMMP; however, we demonstrated that, also in this case, the binding of DMMP occurs, although with a lower binding constant in the case of a molecular sensor.[23]

Considering the excellent results obtained in aqueous solution, we tested the sensorial capabilities of the organic nanostructured sensor under the primary conditions of a real sensor: in air, by exposing to CWA vapors. In particular, the ability of **CNPs-C_2-OH** to detect DMMP with high affinity and sensibility has been investigated with the Test Strip for vapor sensing. To this end, we exposed the functionalized nanoparticles to progressive amounts of DMMP vapors (control tests were performed by using unfunctionalized nanoparticles exposed to the same amounts of the simulant) into a closed vial, for 1h at 50 °C. A clear change of emission intensity was observed under UV irradiation. In particular, 2 μL of a sensor solution (0.05 mg/mL) were properly deposited onto several substrates. No optical response was observed after the exposition to CWA vapors of the functionalized nanoparticles deposited on cellulose paper or silica gel. Conversely, by using a neutral alumina substrate, an increase of the fluorescence intensity was detected. This behavior can be described in terms of interaction with the substrate of the functionalized nanoparticles. It is known that by depositing fluorescent nanostructures onto a solid substrate, surface-induced quenching phenomena may occur.[54,55] This is probably what happens with such OH-rich surfaces of cellulose or silica, which strongly interact with the surface of the organic nanostructure, thus avoiding the possibility to recognize DMMP. By contrast, using neutral alumina, the interaction with the surface will be milder, thus allowing the interaction with the DMMP vapors. The enhancement of the fluorescence emission by the progressive increase of the simulant concentration is ascribable to the shielding effect of DMMP coating on nanoparticles, which limits the interactions with the alumina surface.[54,55] As a result of the formation of the supramolecular complex between the organic nanostructure and the simulant, the photoexcited nanoparticles will find pathways of radioactive relaxation so that they will emit into the visible in an apparent way, as shown in Figure 5.

In order to verify the sensory capabilities as the concentration of CWA vapors increases, we implemented an automatic image processing method allowing to extract quantitative information from the luminance of the spot.

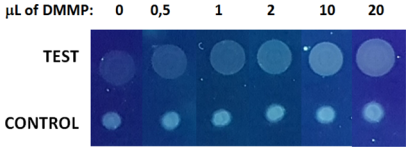

Figure 5. Test Strip vapors: images of 2 mL of **CNPs-C_2-OH** (TEST, 0.05 mg/mL in water) and 2 mL of unfunctionalized carbon nanoparticles (CONTROL, 0.05 mg/mL in water), adsorbed onto neutral alumina foil, exposed to progressive amounts of DMMP for 1 h at 50 °C, and then exposed under UV−vis lamp (365 nm). Pure DMMP does not interfere with the fluorescence enhancement (see Figure S8 of the Supporting Information).

https://dx.doi.org/10.1021/acsanm.0c01593
ACS Appl. Nano Mater. 2020, 3, 8182−8191

Figure 6a shows some region of interest related to fluorescence spots obtained for different concentrations of

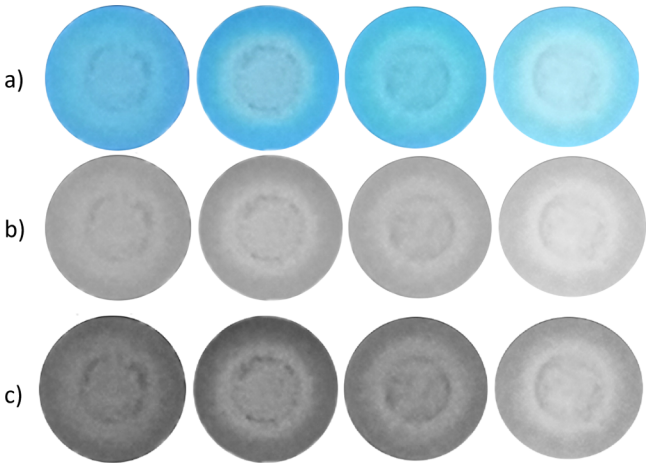

Figure 6. (a) Selected region on interest related to fluorescence spots obtained at different concentrations. From left to right: 0.87, 3.04, 4.00 and 12 ppm. (b) Same in their gray level version. (c) Normalized version.

CWA vapors by using a smartphone to collect these images. As the concentration of the nerve gas increases, the average luminance of the relative image increases, so this feature can be used to discriminate the various gas concentrations. Becasue this feature is preserved in the gray level image version, we transformed the color images into gray level ones (see Figure 6b), thus reducing the computational burden. In order to emphasize the mean luminance difference between the different images, we normalized the gray level image intensity I (see Figure 6c).

Figure 7a reports the relationship between normalized average luminance (A_N) as a function of the normalized

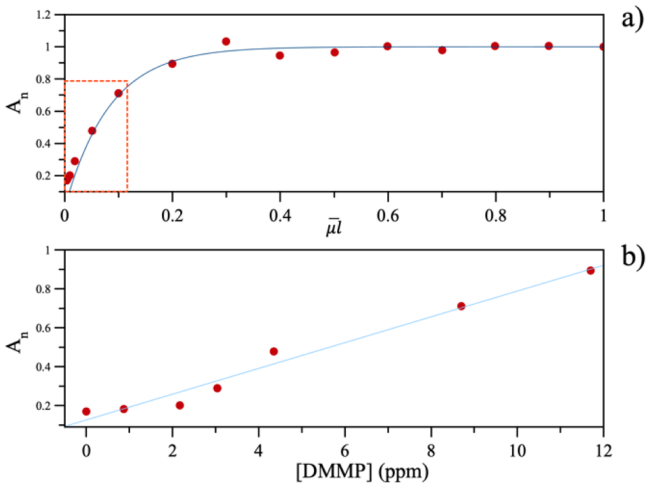

Figure 7. (a) Best fit of the experimental data obtained by using eq 1; (b) magnification of the low concentration region of section (a).

DMMP volume ($\overline{\mu L}$) (see the Experimental section). We found a very good fitting with the equation

$$A_N(\overline{\mu L}) = 1 - e^{-\alpha \cdot \overline{\mu L}} \quad (7)$$

on the set of experimental data available (80 data points), obtaining an average error of about 8%, with $\alpha = 12$. The curve shows that, due to the DMMP vapor saturation of the container used for the Test Strip, at high concentrations the fluorescent spots do not change. Notably, functionalized nanoparticles are able to detect nerve gas vapors even at low concentrations. These low concentration values are, in general, the most important concentration ranges where a sensor should efficiently work. In addition, in this crucial area, a simpler linear relationship can be used between the amount of DMMP to which functional nanoparticles are subjected to and their solid luminescence. Therefore, by means of simple periodic calibration procedures, it would be possible to use the solid device for the quantitative determination of nerve gas. Figure 7b shows the calibration line as experimentally evaluated (expressed in ppm of DMMP vapor presented in the closed box). It is noteworthy that, even in the solid state, it is possible to reach extremely low concentrations to detect even values in the order of ppm or lower.

Recovery tests were performed in order to validate the reversibility of the solid device, guaranteed by the supramolecular approach. Solid devices previously exposed to simulant vapors have been recovered to the initial fluorescence intensity by exposure to moderate high temperature (+80 °C) for 4 h. This temperature value allows to break hydrogen bonds between the nanosensors and the simulant, thus restoring the starting sensor. Intensity emissions recorded after further exposures to the same amount of simulant vapors, as reported in Figure 8, demonstrate the robustness of the sensor adsorbed on the solid support, also after 7 cycles. Figure 9 summarizes the sensing cycles on **CNPs-C_2-OH**.

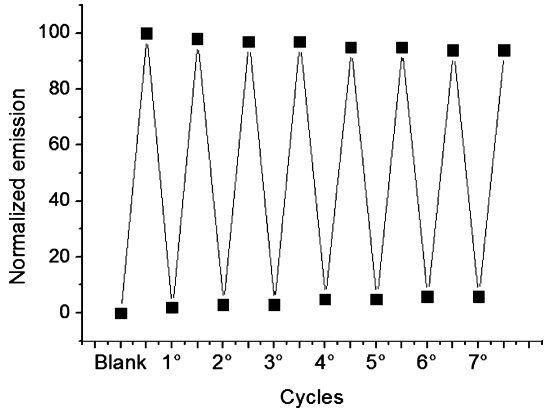

Figure 8. Recovery tests: normalized fluorescence responses of Test Strip to 2 mL of DMMP into a closed 23 mL vial, and successive recovery of the sensor by exposure of the solid device to a temperature of 80 °C for 4 h in an oven.

Because of the similar volatility value of DMMP (5562 mg/m^3 at 25 °C) with respect to the G-type CWAs (Tabun: 576−610 mg/m^3 at 25 °C, Sarin 16,400−22,000 mg/m^3 at 25 °C, Soman 3060−3900 mg/m^3 at 25 °C), this Test Strip can be considered validated also for real Nerve Agents. In addition, the LCt50 (concentration−time product, i.e., lethal to 50% of those exposed and reflects toxicity by the inhalational route) for Tabun, Sarin, and Soman are in the range 1.5−24 ppm × m^3 × h^{-1},[3] thus our nanosensor is able to detect these CWAs in time before the lethal effect.

https://dx.doi.org/10.1021/acsanm.0c01593
ACS Appl. Nano Mater. 2020, 3, 8182−8191

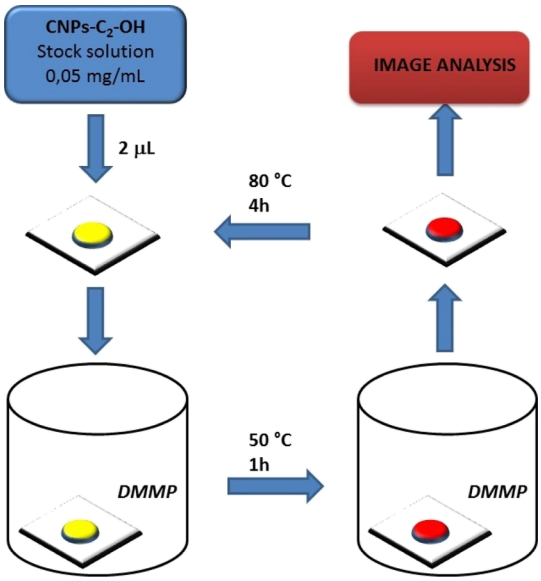

Figure 9. Schematic representation of sensing in gas media performed by **CNPs-C_2-OH**, and successive recovery of the nanoscale sensor.

The International Union of Pure and Applied Chemistry (IUPAC) defines a chemical sensor as a small measurement system that allows the qualitative and quantitative conversion of the chemical information about the presence of the selected analyte.[56] The other known sensors for the detection of CWAs are: (i) mass sensitive, based on the piezoelectric effect, in which the detection limits are in most cases in the order of ppm; (ii) surface acoustic wave chemical sensors, where the analyte detection is related to a change in acoustic frequencies of surface waves; (iii) quartz crystal microbalance sensors, which reach the detection limit of 0.13 ppm of DMMP;and (iv) semiconductor sensors, which are sensitive to a change of resistance in the presence of the anlyte, based on carbon nanotubes, metal oxides, zeolite, and graphene.[57] In all these cases, many technological processes are required, such as photolithography and screen printing. Furthermore, the materials (silicons, geramics and polymer) and the technologies required to realize the above-mentioned sensors are expensive. Here, we propose a prototype, based on easily functionalized carbon nanoparticles, adsorbed onto aluminum foil.

4. CONCLUSIONS

A new nanostructured sensor for the simultaneous detection of nerve agents in air and water, based on carbon nanoparticles functionalized with ethanolamine arms, has been synthesized and characterized by NMR, AFM, XPS, and TEM. The ability to detect DMMP, a CWA simulant, both in solution and in the gas phase has been demonstrated by fluorescence spectroscopy. In particular, the supramolecular approach here proposed allow us to obtain an efficient sensor (log 6.46), having high selectivity for the selected target analyte. Notably, the limit of detection in solution is lower than the ppt levels. Solid devices obtained by the simple deposition of nanoparticles onto neutral alumina foil, which are able to detect the presence of sub-ppm levels of the simulant in the gas phase smartphone or a digital camera, can be recovered at least 7 times. Because of the LC50 values, Sarin (1.2 ppm), Soman (0.9 ppm), and VX (0.3 ppm),[3] our nanosensor is able to detect amounts of NAs much lower than these values. In addition, the IDLH values of these NAs (the concentration of toxin, i.e., immediately dangerous for life and health) are 0.03 ppm for Tabun and Sarin, 8 ppb for Soman, and 2 ppb for VX. Also in this case, the nanosensor here reported can efficiently recognize lower levels, by standing as an efficient real device to detect the chemical warning in a terrorist attack. By changing the functionalization of the external shell of the nanoparticle, we are working to realize selective supramolecular nanosensors for V-Type of CWAs, which require the noncovalent recognition of longer aliphatic chains with respect to the G-Type.

■ ASSOCIATED CONTENT

Supporting Information

The Supporting Information is available free of charge at https://pubs.acs.org/doi/10.1021/acsanm.0c01593.

NMR, AFM, XPS, and FTIR characterization, fluorescence titrations, and selectivity tests (PDF)

■ AUTHOR INFORMATION

Corresponding Authors

Nunzio Tuccitto − *Department of Chemical Sciences, University of Catania, 95125 Catania, Italy; Laboratory for Molecular Surfaces and Nanotechnology−CSGI, 95125 Catania, Italy;* orcid.org/0000-0003-4129-0406; Email: n.tuccitto@unict.it

Giuseppe Trusso Sfrazzetto − *Department of Chemical Sciences, University of Catania, 95125 Catania, Italy; National Interuniversity Consortium for Materials Science and Technology (I.N.S.T.M.) Research Unit of Catania, 95125 Catania, Italy;* orcid.org/0000-0003-1584-5869; Email: giuseppe.trusso@unict.it

Authors

Lorenzo Riela − *Department of Chemical Sciences, University of Catania, 95125 Catania, Italy*

Agatino Zammataro − *Department of Chemical Sciences, University of Catania, 95125 Catania, Italy*

Luca Spitaleri − *Department of Chemical Sciences, University of Catania, 95125 Catania, Italy; National Interuniversity Consortium for Materials Science and Technology (I.N.S.T.M.) Research Unit of Catania, 95125 Catania, Italy;* orcid.org/0000-0001-7020-9721

Giovanni Li-Destri − *Department of Chemical Sciences, University of Catania, 95125 Catania, Italy; Laboratory for Molecular Surfaces and Nanotechnology−CSGI, 95125 Catania, Italy;* orcid.org/0000-0001-6195-659X

Gianfranco Sfuncia − *Department of Chemical Sciences, University of Catania, 95125 Catania, Italy*

Giuseppe Nicotra − *Department of Chemical Sciences, University of Catania, 95125 Catania, Italy*

Andrea Pappalardo − *Department of Chemical Sciences, University of Catania, 95125 Catania, Italy; National Interuniversity Consortium for Materials Science and Technology (I.N.S.T.M.) Research Unit of Catania, 95125 Catania, Italy*

Giacomo Capizzi − *Department of Electrical, Electronics and Informatics Engineering, University of Catania, 95125 Catania, Italy*

Complete contact information is available at: https://pubs.acs.org/10.1021/acsanm.0c01593

https://dx.doi.org/10.1021/acsanm.0c01593
ACS Appl. Nano Mater. 2020, 3, 8182−8191

Author Contributions

L.R. and A.Z. performed the synthesis and functionalization of the nanosensor; L.S. performed XPS experiments, G.L.-D. performed AFM analysis; G.S. and G.N. performed TEM analysis; A.P. analyzed data; G.C. performed image analysis; and N.T. and G.T.S. designed experiments and wrote the paper. All the authors have given approval to the final version of the manuscript.

Funding

Università degli Studi di Catania, Piano della Ricerca di Ateneo 2016−2018 and NaTI4Smart PIACERI 2020 call.

Notes

The authors declare no competing financial interest.

■ ACKNOWLEDGMENTS

The authors acknowledge Prof. Giovanni Marletta for helpful debate and inspiring conversations, and Prof. Antonino Gulino for his valuable suggestions on the data treatment. The authors also thank Dr. Luca Fichera for the support in the nanoparticle's synthesis, and the University of Catania (Piano della Ricerca di Ateneo 2016−2018) for financial support. N.T. acknowledge NaTI4Smart project for partial funding.

■ REFERENCES

(1) Stone, R. U.K. attack puts nerve agent in the spotlight. *Science* **2018**, *359*, 1314−1315.
(2) Stone, R. How to defeat a nerve agent. *Science* **2018**, *359*, 23.
(3) Wiener, S. W.; Hoffman, R. S. Nerve Agents: A Comprehensive Review. *J. Intensive Care Med.* **2004**, *19*, 22−37.
(4) Lavoie, J.; Srinivasan, S.; Nagarajan, R. Using cheminformatics to find simulants for chemical warfare agents. *J. Hazard. Mater.* **2011**, *194*, 85−91.
(5) Jang, Y. J.; Kim, K.; Tsay, O. G.; Atwood, D. A.; Churchill, D. G. Update 1 of: Destruction and detection of Chemical Warfare Agents. *Chem. Rev.* **2015**, *115*, PR1−PR76.
(6) Zhou, X.; Lee, S.; Xu, Z.; Yoon, J. Recent progress on the development of chemosensors for gases. *Chem. Rev.* **2015**, *115*, 7944−8000.
(7) Sambrook, M. R.; Notman, S. Supramolecular chemistry and chemical warfare agents: from fundamentals of recognition to catalysis and sensing. *Chem. Soc. Rev.* **2013**, *42*, 9251−9267.
(8) Hiscock, J. R.; Piana, F.; Sambrook, M. R.; Wells, N. J.; Clark, A. J.; Vincent, J. C.; Busschaert, N.; Brown, R. C. D.; Gale, P. A. Detection of nerve agent via perturbation of supramolecular gel formation. *Chem. Commun.* **2013**, *49*, 9119−9121.
(9) Tudisco, C.; Betti, P.; Motta, A.; Pinalli, R.; Bombaci, L.; Dalcanale, E.; Condorelli, G. G. Cavitand-Functionalized Porous Silicon as an Active Surface for Organophosphorus Vapor Detection. *Langmuir* **2012**, *28*, 1782−1789.
(10) Barba-Bon, A.; Costero, A. M.; Parra, M.; Gil, S.; Martínez-Máñez, R.; Sancenón, F.; Gale, P. A.; Hiscock, J. R. Neutral 1,3-Diindolylureas for Nerve Agent Remediation. *Chem.—Eur. J.* **2013**, *19*, 1586−1590.
(11) Sambrook, M. R.; Hiscock, J. R.; Cook, A.; Green, A. C.; Holden, I.; Vincent, J. C.; Gale, P. A. Hydrogen bond-mediated recognition of the chemical warfare agent soman (GD). *Chem. Commun.* **2012**, *48*, 5605−5607.
(12) Chen, S.; Ruan, Y.; Brown, J. D.; Gallucci, J.; Maslak, V.; Hadad, C. M.; Badjić, J. D. Assembly of Amphiphilic Baskets into Stimuli-Responsive Vesicles. Developing a Strategy for the Detection of Organophosphorus Chemical Nerve Agents. *J. Am. Chem. Soc.* **2013**, *135*, 14964−14967.
(13) Ruan, Y.; Dalkiliç, E.; Peterson, P. W.; Pandit, A.; Dastan, A.; Brown, J. D.; Polen, S. M.; Hadad, C. M.; Badjić, J. D. Trapping of Organophosphorus Chemical Nerve Agents in Water with Amino Acid Functionalized Baskets. *Chem.—Eur. J.* **2014**, *20*, 4251−4256.
(14) Chen, S.; Ruan, Y.; Brown, J. D.; Hadad, C. M.; Badjić, J. D. Recognition Characteristics of an Adaptive Vesicular Assembly of Amphiphilic Baskets for Selective Detection and Mitigation of Toxic Nerve Agents. *J. Am. Chem. Soc.* **2014**, *136*, 17337−17342.
(15) Ruan, Y.; Chen, S.; Brown, J. D.; Hadad, C. M.; Badjić, J. D. Ubiquitous Assembly of Amphiphilic Baskets into Unilamellar Vesicles and Their Recognition Characteristics. *Org. Lett.* **2015**, *17*, 852−855.
(16) Moon, S.-Y.; Liu, Y.; Hupp, J. T.; Farha, O. K. Instantaneous Hydrolysis of Nerve-Agent Simulants with a Six-Connected Zirconium-Based Metal−Organic Framework. *Angew. Chem., Int. Ed.* **2015**, *54*, 6795−6799.
(17) Mondloch, J. E.; Katz, M. J.; Isley III, W. C., III; Ghosh, P.; Liao, P.; Bury, W.; Wagner, G. W.; Hall, M. G.; DeCoste, J. B.; Peterson, G. W.; Snurr, R. Q.; Cramer, C. J.; Hupp, J. T.; Farha, O. K. Destruction of chemical warfare agents using metal−organic frameworks. *Nat. Mater.* **2015**, *14*, 512−516.
(18) Pappalardo, A.; Amato, M. E.; Ballistreri, F. P.; La Paglia Fragola, V.; Tomaselli, G. A.; Toscano, R. M.; Trusso Sfrazzetto, G. Binding of Reactive Organophosphate by Oximes via Hydrogen Bond. *J. Chem. Sci.* **2013**, *125*, 896−873.
(19) Sfrazzetto, G. T.; Millesi, S.; Pappalardo, A.; Tomaselli, G. A.; Ballistreri, F. P.; Toscano, R. M.; Fragalà, I.; Gulino, A. Nerve Gas Simulant Sensing by an Uranyl-Salen Monolayer Covalently Anchored on Quartz Substrates. *Chem.—Eur. J.* **2017**, *23*, 1576−1583.
(20) Puglisi, R.; Ballistreri, F. P.; Gangemi, C. M. A.; Toscano, R. M.; Tomaselli, G. A.; Pappalardo, A.; Sfrazzetto, G. T. Chiral Zn−salen complexes: a new class of fluorescent receptors for enantiodiscrimination of chiral amines. *New J. Chem.* **2017**, *41*, 911−915.
(21) Puglisi, R.; Mineo, P. G.; Pappalardo, A.; Gulino, A.; Trusso Sfrazzetto, G. Supramolecular Detection of a Nerve Agent Simulant by Fluorescent Zn−Salen Oligomer Receptors. *Molecules* **2019**, *24*, 2160.
(22) Puglisi, R.; Pappalardo, A.; Gulino, A.; Trusso Sfrazzetto, G. Supramolecular recognition of CWAs simulant by metal-salen complexes: the first multi-topic approach. *Chem. Commun.* **2018**, *54*, 11156−11159.
(23) Puglisi, R.; Pappalardo, A.; Gulino, A.; Trusso Sfrazzetto, G. Multitopic Supramolecular Detection of Chemical Warfare Agents by Fluorescent Sensors. *ACS Omega* **2019**, *4*, 7550−7555.
(24) Legnani, L.; Puglisi, R.; Pappalardo, A.; Chiacchio, M. A.; Trusso Sfrazzetto, G. Supramolecular recognition of phosphocholine by an enzyme-like cavitand receptor. *Chem. Commun.* **2020**, *56*, 539−542.
(25) Briggs, D.; Grant, J. T. *Surface Analysis by Auger and X-Ray Photoelectron Spectroscopy*; Surface Spectra Ltd.: Manchester, U.K. 2003.
(26) Gulino, A. Structural and electronic characterization of self-assembled molecular nanoarchitectures by X-ray photoelectron spectroscopy. *Anal. Bioanal. Chem.* **2013**, *405*, 1479−1495.
(27) Zammataro, A.; Gangemi, C. M. A.; Pappalardo, A.; Toscano, R. M.; Puglisi, R.; Nicotra, G.; Fragalà, M. E.; Tuccitto, N.; Sfrazzetto, G. T. Covalently functionalized carbon nanoparticles with a chiral Mn-Salen: a new nanocatalyst for enantioselective epoxidation of alkenes. *Chem. Commun.* **2019**, *55*, 5255−5258.
(28) Pappalardo, A.; Amato, M. E.; Ballistreri, F. P.; Tomaselli, G. A.; Toscano, R. M.; Trusso Sfrazzetto, G. Pair of Diastereomeric Uranyl Salen Cavitands Displaying Opposite Enantiodiscrimination of α-Amino Acid Ammonium Salts. *J. Org. Chem.* **2012**, *77*, 7684−7687.
(29) Pappalardo, A.; Ballistreri, F. P.; Destri, G. L.; Mineo, P. G.; Tomaselli, G. A.; Toscano, R. M.; Trusso Sfrazzetto, G. Supramolecular Polymer Networks Based on Calix[5]arene Tethered Poly(p-phenyleneethynylene). *Macromolecules* **2012**, *45*, 7549−7556.
(30) Ballistreri, F. P.; Pappalardo, A.; Tomaselli, G. A.; Toscano, R. M.; Sfrazzetto, G. T. Heteroditopic Chiral Uranyl-Salen Receptor for

https://dx.doi.org/10.1021/acsanm.0c01593
ACS Appl. Nano Mater. 2020, 3, 8182−8191

Molecular Recognition of Amino Acid Ammonium Salts. *Eur. J. Org. Chem.* **2010**, 3806−3810.
(31) Amato, M. E.; Ballistreri, F. P.; D'Agata, S.; Pappalardo, A.; Tomaselli, G. A.; Toscano, R. M.; Sfrazzetto, G. T. Enantioselective Molecular Recognition of Chiral Organic Ammonium Ions and Amino Acids Using Cavitand-Salen Based Receptors. *Eur. J. Org. Chem.* **2011**, 5674−5680.
(32) Guo, X.; Qian, X.; Jia, L. A Highly Selective and Sensitive Fluorescent Chemosensor for Hg2+ in Neutral Buffer Aqueous Solution. *J. Am. Chem. Soc.* **2004**, *126*, 2272−2273.
(33) Butrow, A. B.; Buchanan, J. H.; Tevault, D. E. Vapor Pressure of Organophosphorus Nerve Agent Simulant Compounds. *J. Chem. Eng. Data* **2009**, *54*, 1876−1883.
(34) Baptista, F. R.; Belhout, S. A.; Giordani, S.; Quinn, S. J. Recent developments in carbon nanomaterial sensors. *Chem. Soc. Rev.* **2015**, *44*, 4433−4453.
(35) Qu, S.; Chen, H.; Zheng, X.; Cao, J.; Liu, X. Ratiometric fluorescent nanosensor based on water soluble carbon nanodots with multiple sensing capacities. *Nanoscale* **2013**, *5*, 5514−5518.
(36) Zhu, A.; Qu, Q.; Shao, X.; Kong, B.; Tian, Y. Carbon-Dot-Based Dual-Emission Nanohybrid Produces a Ratiometric Fluorescent Sensor for In Vivo Imaging of Cellular Copper Ions. *Angew. Chem., Int. Ed.* **2012**, *51*, 7185−7189.
(37) Licciardello, N.; Hunoldt, S.; Bergmann, R.; Singh, G.; Mamat, C.; Faramus, A.; Ddungu, J. L. Z.; Silvestrini, S.; Maggini, M.; De Cola, L.; Stephan, H. Biodistribution studies of ultrasmall silicon nanoparticles and carbon dots in experimental rats and tumor mice. *Nanoscale* **2018**, *10*, 9880−9891.
(38) Wang, H.; Cao, G.; Gai, Z.; Hong, K.; Banerjee, P.; Zhou, S. Magnetic/NIR-responsive drug carrier, multicolor cell imaging, and enhanced photothermal therapy of gold capped magnetite-fluorescent carbon hybrid nanoparticles. *Nanoscale* **2015**, *7*, 7885−7895.
(39) Li-Destri, G.; Fichera, L.; Zammataro, A.; Trusso Sfrazzetto, G.; Tuccitto, N. Self-Assembled Carbon Nanoparticles as Messengers for Artificial Chemical Communication. *Nanoscale* **2019**, *11*, 14203−14209.
(40) Habisreutinger, S. N.; Schmidt-Mende, L.; Stolarczyk, J. K. Photocatalytic Reduction of CO2 on TiO2 and Other Semiconductors. *Angew. Chem., Int. Ed.* **2013**, *52*, 7372−7408.
(41) Gulino, A.; Mineo, P.; Scamporrino, E.; Vitalini, D.; Fragalà, I. Spectroscopic and Microscopic Characterization and Behavior of an Optical pH Meter Based on a Functional Hybrid Monolayer Molecular System: Porphyrin Molecules Covalently Assembled on a Molecularly Engineered Silica Surface. *Chem. Mater.* **2006**, *18*, 2404−2410.
(42) Contino, A.; Maccarrone, G.; Spitaleri, L.; Torrisi, L.; Nicotra, G.; Gulino, A. One Pot Synthesis of Au_ZnO Core-Shell Nanoparticles Using a Zn Complex Acting as ZnO Precursor, Capping and Reducing Agent During the Formation of Au NPs. *Eur. J. Inorg. Chem.* **2018**, 4678−4683.
(43) Spitaleri, L.; Nicotra, G.; Zimbone, M.; Contino, A.; Maccarrone, G.; Alberti, A.; Gulino, A. Fast and Efficient Sun Light Photocatalytic Activity of Au_ZnO Core-Shell Nanoparticles Prepared by a One-Pot Synthesis. *ACS Omega* **2019**, *4*, 15061−15066.
(44) Parvizi, R.; Azad, S.; Dashtian, K.; Ghaedi, M.; Heidari, H. Natural Source-Based Graphene as Sensitising Agents for Air Quality Monitoring. *Sci. Rep.* **2019**, *9*, 3798.
(45) Ding, Y.; Zhang, F.; Xu, J.; Miao, Y.; Yang, Y.; Liu, X.; Xu, B. Synthesis of short-chain passivated carbon quantum dots as the light emitting layer towards electroluminescence. *RSC Adv.* **2017**, *7*, 28754−28762.
(46) Graf, N.; Yegen, E.; Gross, T.; Lippitz, A.; Weigel, W.; Krakert, S.; Terfort, A.; Unger, W. E. S. XPS and NEXAFS studies of aliphatic and aromatic amine species on functionalized surfaces. *Surf. Sci.* **2009**, *603*, 2849−2860.
(47) Liu, Y.; Yu, Z.-L.; Zhang, Y.-M.; Guo, D.-S.; Liu, Y.-P. Supramolecular Architectures of β-Cyclodextrin-Modified Chitosan and Pyrene Derivatives Mediated by Carbon Nanotubes and Their DNA Condensation. *J. Am. Chem. Soc.* **2008**, *130*, 10431−10439.
(48) Kancharla, S.; Sasaki, K. Acid tolerant covalently functionalized graphene oxide for the selective extraction of Pd from highlevel radioactive liquid wastes. *J. Mater. Chem. A* **2019**, *7*, 4561−4573.
(49) Ding, H.; Yu, S.-B.; Wei, J.-S.; Xiong, H.-M. Full-Color Light-Emitting Carbon Dots with a Surface-State-Controlled Luminescence Mechanism. *ACS Nano* **2016**, *10*, 484−491.
(50) Zhang, Y.; Cui, P.; Zhang, F.; Feng, X.; Wang, Y.; Yang, Y.; Liu, X. Fluorescent probes for "off-on" highly sensitive detection of Hg2+ and L-cysteine based on nitrogen-doped carbon dots. *Talanta* **2016**, *152*, 288−300.
(51) XPS analysis revealed a nanoparticle composition of C 67, O 19.7 and N 13.3%. Thus, the carbon contribution of ethanolamine is 26.6%. Considering that, each graphene layer contains ca. 68 fused aromatic rings, each nanoparticle contains ca. 2720 carbon atoms, of which 1725 derived from ethanolmine arms. Taking into account these considerations, the average number of ethanolamine molecules onto the surface is 860. Considering that the average area of a nanoparticle, obtained combining TEM and AFM data, is 476 nm^2, due to the footprint of an ethanolamine molecule (0.28 nm^2), each nanoparticle can accommodate ca. 1700 molecules of ethanolamine arms. We note that, by the contrast respect to metal nanoparticles, carbon nanoparticles cannot be fully functionalizable in their external shell. Thus, the coverage here obtained is high.
(52) Trusso Sfrazzetto, G.; Satriano, C.; Tomaselli, G. A.; Rizzarelli, E. Synthetic fluorescent probes to map metallostasis and intracellular fate of zinc and copper. *Coord. Chem. Rev.* **2016**, *311*, 125−167.
(53) The estimated concentration of the ethanolamine arms on the surface nanoparticle has been carried out considering an average of 860 molecules onto the nanoparticles. This value leads to an apparent molecular mass of 51,600 Da and an apparent concentration of 1.0×10^{-6} M in the cuvette.
(54) Xu, J.; Sahu, S.; Cao, L.; Bunker, C. E.; Peng, G.; Liu, Y.; Fernando, K. A. S.; Wang, P.; Guliants, E. A.; Meziani, M. J.; Qian, H.; Sun, Y.-P. Efficient Fluorescence Quenching in Carbon Dots by Surface-Doped Metals - Disruption of Excited State Redox Processes and Mechanistic Implications. *Langmuir* **2012**, *28*, 16141−16147.
(55) Demchenko, A. P.; Dekaliuk, M. O. The origin of emissive states of carbon nanoparticles derived from ensemble-averaged and single-molecular studies. *Nanoscale* **2016**, *8*, 14057−14069.
(56) Hulanicki, A.; Glab, S.; Ingman, F. Chemical Sensors: definitions and Classification. *Pure Appl. Chem.* **1991**, *63*, 1247−1250.
(57) Bielecki, M.; Witkiewicz, Z.; Rogala, P. Sensors to Detect Sarin Simulant. *Crit. Rev. Anal. Chem.* **2020**, 1−13.

https://dx.doi.org/10.1021/acsanm.0c01593
ACS Appl. Nano Mater. 2020, 3, 8182−8191